Control of High Density Microcantilever Systems

BERKEM MEHMET
MBtech Group
Powertrain
Salierstr. 21, 70736 Fellbach
GERMANY
berkem.mehmet@mbtech-group.com

HUSSAM SEHWAIL
ITC Holdings
ITC Transmission
27175 Energy Way, 48377 Novi
USA
hsehwail@itctransco.com

PETROS G. VOULGARIS
University of Illinois
Aerospace Engineering
161 CSL, 61801 Urbana
USA
voulgari@illinois.edu

Abstract: In this paper we build on our earlier work on the control of high density, electrostatically actuated, microcantilever arrays and present simple state feedback controllers that can achieve reasonable performance. These controllers are localized, spatially distributed and yield tracking performances comparable to the performance of the distributed H_∞ controller proposed in our earlier study, for reference frequencies as high as 3000 rad/sec. These simpler structures come with the cost of worse performance at higher frequencies, relatively inferior robustness to phase shifts and a state availability requirement. Therefore, it can be effectively used for relatively lower bandwidth applications where the states are measurable. The above results are further verified by using a multimodal model of the cantilever system.

Key–Words: AFM, Multivariable Systems, Distributed Control, Finite Element Method.

1 Introduction

The cantilever is a classical engineering structure whose motion has been heavily studied and is fairly well understood. Put simply, a cantilever is merely a beam that is held rigid at one end. Nanotechnology has led to the creation of microcantilevers. These small scale mechanical structures can be made of materials that can actuate the cantilevers' bending using a voltage. This allows the control and measurement of the beams' microscopic bending and allows for various scientific and industrial applications.

The importance of microcantilevers in the scientific field has been clear since the advent of the atomic force microscope (AFM). While the scanning tunneling microscope was a huge breakthrough, it had serious limitations with regards to observable materials, necessary environments and isolating force effects, which could not be addressed until the invention of the AFM in 1986 by Binnig, Quate, and Gerber [4]. Five years later the AFM was used to show atomic resolution of inert surfaces and there are now thousands of AFMs being used in research labs [4] and numerous other applications over the years. Due to the prevalence of relatively low-cost AFM cantilevers, the interest in microcantilever sensors in detecting surface stress was revived [9].

Microcantilevers have demonstrated success in a variety of sensor applications. They have been able to image and detect biological structures including DNA and proteins [3, 9]. More generally, arrays of piezoelectric microcantilevers can be specially coated and respond to particular substances with the bending response thereby causing a change in voltage resulting in sensitive chemical detectors [15]. Microcantilevers can also be used to detect particular bands of electromagnetic waves, and may serve as more affordable substitutes to current detectors [14]. Additionally, there is the potential for fast, high-density data storage applications, and small scale chips have already been fabricated [2].

This paper, leveraging on our previous work in [12] and [11], and our work in [8], presents a spatially invariant model of a system of very closely spaced microcantilevers that can be capacitively actuated and sensed independently, and tests it with various controllers. The tests are performed with respect to tracking performance and stability properties. The first one of the controllers is a state feedback, decentralized (meaning each cantilever has its own controller and the controller does not communicate with its neighbors) velocity feedforward controller with a PID component. The second controller is a distributed (meaning each cantilever has its own controller and the controller communicates with the immediate neighbors only), state feedback LQR controller from [5] that is designed with simultaneous localization and optimization. The state feedback controllers are easy to implement, do not involve many calculations and provide quite satisfactory results. Distributed H_∞ controller is the main alternative for the cases where the displacements of the cantilevers are not measurable.

In order to obtain a more accurate picture, the control tests are also performed with a more complex, multimodal modeling of the system.

The paper is organized as follows: In Section 2 modeling and description of the system is presented. This is followed by showing the feedforward, LQR and the H_∞ controller designs and their simulation results in Section 3. In Section 4 the multimodal model of the system and the results with the previous controllers are presented. The robustness of the system with respect to different parameters is discussed in Section 5. Finally, the paper is concluded with comments and discussion of future work.

2 System Modeling

2.1 Core Model

The microcantilevers considered in this paper are capacitively actuated plates, with one rigid plate at the bottom and one more flexible plate at the top as shown in Figure 1. The top plate is rigid in horizontal direction and can move in vertical direction only. The vertical displacement of each microcantilever is controlled by applying a voltage across the plates. The system model consists of an infinite number of these cantilevers located in quite close proximity to each other connected to a base. Therefore, despite each microcantilever's being actuated independently, its dynamics are influenced by the presence of other microcantilevers. This influence has two sources: First one is the mechanical coupling because of microcantilevers' being attached to the same base and the second one is the electrical coupling due to the electromagnetic forces applied by the neighboring micro-capacitors. The system with the coupling effects are depicted in Figure 2. Regarding these the equation of motion for a single cantilever can be written as:

$$\ddot{z_i} + b\dot{z_i} + kz_i = F_{a,i} + F_{mech,i} + F^{\perp}_{elec,i} \qquad (1)$$

In this equation the subscripts i refer to which cantilever the equation describes. For cantilever i, the symbol z_i is the vertical displacement of the cantilever tip, b is the normalized damping coefficient and k is the conceptual spring constant. The spring constant can be rewritten as $k = \omega^2$ with ω being the natural resonant frequency of the i_{th} cantilever. $F_{a,i}$ is the force of attraction between the tip of cantilever i and the rigid plate below it. The cantilever's and the rigid plate's acting as electrodes across which voltage is produced cause electrostatic attraction between them having the following formula:

$$F_{a,i} = \frac{\epsilon_0 A}{2md^2}(1 + \frac{2z_i}{d})V_i^2 \qquad (2)$$

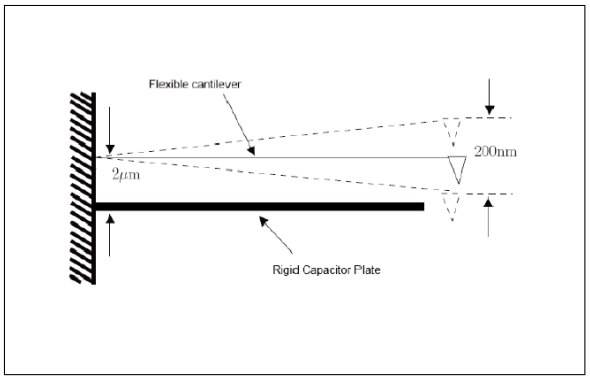

Figure 1: A side view of a single cantilever and its respective plate. The cantilever shows a range of vertical motion [12]

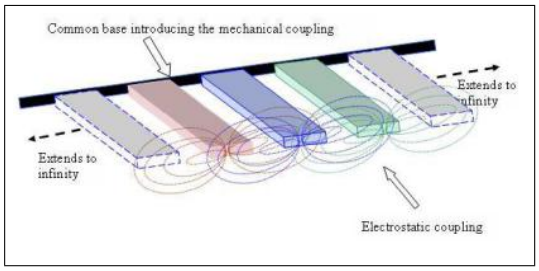

Figure 2: Layout of the infinite dimensional microcantilever array with mechanical and electrostatic coupling [12]

where ϵ_0 is the permittivity of vacuum, A is the area of the cantilever (length by width), d is the gap between the cantilever and the rigid plate below, m is the mass of the cantilever and V_i is the voltage across the electrodes of cantilever i.

The mechanical coupling, F_{mech}, can be modeled like a spring force between the bases of the cantilevers. Only the immediate neighbors have a significant mechanical influence on the cantilever and this force is proportional to the difference between the position of the cantilever tip and that of its immediate neighbor. The mechanical coupling can be modeled as follows:

$$F_{mech,i} = \frac{1}{m} \sum_{j=i-1, j\neq i}^{i+1} \gamma_{i,j}(z_j - z_i) \qquad (3)$$

where γ is the mechanical coupling coefficient.The index j refers to the neighboring cantilever.

Finally $F^{\perp}_{elec}$ is the electrostatic coupling between a cantilever and its neighbors. Unlike the mechanical coupling, this coupling force is not only generated by the immediate neighbors but by every cantilever in the array. The coupling is determined as in [12] by defining the capacitance c_i of the i_{th} cantilever as:

$$c_i = \epsilon_0 \frac{A}{d - z_i} \qquad (4)$$

using Coulomb's law:

$$F_{elec} = \frac{c_i V_i}{4\pi\epsilon_0} \sum_{j=-\infty, j\neq i}^{\infty} \frac{c_j V_j}{r_{i,j}^2} \quad (5)$$

and finally taking the approximation of the vertical component:

$$F_{elec}^{\perp} \approx \frac{c_i V_i}{4\pi\epsilon_0} \sum_{j=-\infty, j\neq i}^{\infty} \frac{c_j V_j (z_i - z_j)}{r_{i,j}^3} \quad (6)$$

where $r_{i,j}$ is the horizontal distance between cantilevers i and j, as measured from the centroids.

2.2 Linearization

The states of the system are $x_{i,1}$:=z_i for the displacement of the cantilever, $x_{i,2}$:=$\dot{z}_i$ for the velocity of the cantilever, $x_{i,3}$:=V_i for the applied voltage on the cantilever. The state equations are formed as follows:

$$\dot{x}_{i,1} = x_{i,2}$$
$$\dot{x}_{i,2} = -bx_{i,2} - \omega^2 x_{i,1} + F_{a,i} + F_{mech,i} + F_{elec,i}^{\perp} \quad (7)$$

The nonlinear system of the microcantilever array is linearized around its equilibrium point that is

$$x_{e1} = \frac{\epsilon_0 A V_e^2 d}{2(\omega^2 m d^3 - \epsilon_0 A V_e^2)} \quad (8)$$

The mechanical coupling is already linear so it does not need to be changed. The linearization of other driving forces around the equilibrium point is:

$$\widetilde{F}_{a,i} = (\frac{\epsilon_0 d A V_e + 2\epsilon_0 A x_{e1} V_e}{m d^3}) V_i + \frac{\epsilon_0 A V_e^2}{m d^3} x_{i,1} \quad (9)$$

for the force of attraction,

$$\widetilde{F}_{elec,i}^{\perp} = (1 + \frac{x_{e1}^2}{d^2} + \frac{2x_{e1}}{d}) \cdot \epsilon_0 \frac{A^2 V_e^2}{4md^2\pi} \sum_{j=-\infty, j\neq i}^{\infty} \frac{(x_{i,1} - x_{j,1})}{r_{i,j}^3} \quad (10)$$

for the electrical coupling.

The current produced from the bending of the cantilever beams can be defined as the system output that is one of the inputs to the H_∞ controller. It is calculated as:

$$y_i = \mathrm{d}\frac{c_i V_i}{\mathrm{dt}} = \frac{V_i \epsilon_0 A}{d^2} \dot{x}_{i,1} + \frac{\epsilon_0 A}{d} \dot{V}_i + \frac{\epsilon_0 A x_{i,1}}{d^2} \dot{V}_i \quad (11)$$

This equation of output can be linearized as below:

$$y_i = \frac{V_e \epsilon_0 A}{d^2} x_{i,2} + \dot{V}_i \left(\frac{\epsilon_0 A}{d} + \frac{\epsilon_0 A x_{e1}}{d^2} \right) \quad (12)$$

2.3 Matrix Formulation

The nonlinearities in the equations were linearized in the previous section resulting in the following linear system:

$$\begin{aligned}
\dot{x}_{i,1} &= x_{i,2} \\
\dot{x}_{i,2} &= -bx_{i,2} - x_{i,1}\left(\omega^2 - \frac{\epsilon_0 A V_e^2}{m d^3}\right) \\
&+ \left(\frac{\epsilon_0 d A V_e + 2\epsilon_0 A x_{e1} V_e}{m d^3}\right) V_i \\
&+ \frac{1}{m} \sum_{j=i-1, j\neq i}^{i+1} \gamma_{i,j} (\delta x_{1ji}) \\
&- \left(1 + \frac{x_{e1}^2}{d^2} + \frac{2x_{e1}}{d}\right) \frac{\epsilon_0 A^2 V_e^2}{4md^2\pi} \sum_{j=-\infty, j\neq i}^{\infty} \frac{\delta x_{1ji}}{r_{i,j}^3} \\
\dot{x}_{i,3} &= u_i
\end{aligned} \quad (13)$$

with u_i being the input to the i_{th} cantilever and $\delta x_{1ji} = x_{j,1} - x_{i,1}$. The states' coefficients corresponding to driving forces seem to be quite long and complicated. However, they are actually constants so the above linear model equations can be written as:

$$\begin{aligned}
\dot{x}_{i,2} &= -bx_{i,2} - C_1 x_{i,1} + C_2 V_i \\
&+ \sum_{j=i-1, j\neq i}^{i+1} C_3 (\delta x_{1ji}) \\
&- C_4 \left(\sum_{j=-\infty, j\neq i}^{\infty} \frac{\delta x_{1ji}}{r_{i,j}^3} \right)
\end{aligned} \quad (14)$$

where C_1, C_2, C_3, C_4 are constants corresponding to the coefficients in (13).

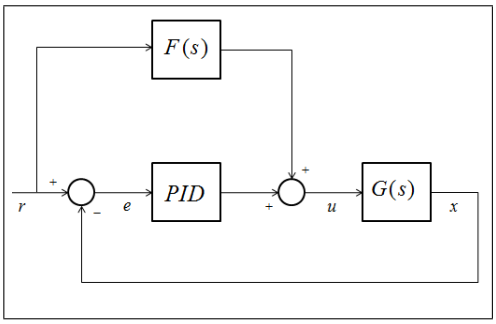

Figure 3: Block Diagram for the Feedforward Controller

The above equations can be written in terms of matrices. For the linear system one obtains the classical state space equation $\dot{x} = Ax + Bu$. For an n-

cantilever system the $3n \times 3n$ state matrix has the following form:

$$\begin{bmatrix} 0 & 1 & 0 & 0 & 0 & 0 & 0 & 0 & 0 \\ a_{21} & -b & a_{23} & EC & 0 & 0\cdots & E_{n-1} & 0 & 0 \\ 0 & 0 & 0 & 0 & 0 & 0 & 0 & 0 & 0 \\ 0 & 0 & 0 & 0 & 1 & 0 & 0 & 0 & 0 \\ EC & 0 & 0 & a_{21} & -b & a_{23}\cdots & E_{n-2} & 0 & 0 \\ 0 & 0 & 0 & 0 & 0 & 0 & 0 & 0 & 0 \\ \vdots & & & & & \ddots & \vdots & & \\ 0 & 0 & 0 & 0 & 0 & 0 & 0 & 1 & 0 \\ E_{n-1} & 0 & 0 & E_{n-2} & 0 & 0\cdots & a_{21} & -b & a_{23} \\ 0 & 0 & 0 & 0 & 0 & 0 & 0 & 0 & 0 \end{bmatrix}$$

where $a_{21} = -C_1 - 2C_3 + E_{total}$, $E_{total} = C_4\left(\sum_{j=-\infty, j\neq i}^{\infty} 1/r_{i,j}^3\right)$, $E_{|i-j|} = -C_4/r_{i,j}^3$, $EC = E_1 + C_3$ and $a_{23} = C_2$. The 3×3 submatrices in the diagonal represent the matrix for the i_{th} cantilever and the other submatrices are their neighbors. Similarly the $3n \times n$ input matrix has the form below:

$$B = \begin{bmatrix} \hat{b} & 0_{3\times1} & \cdots & 0_{3\times1} \\ 0_{3\times1} & \hat{b} & \cdots & 0_{3\times1} \\ \vdots & & \ddots & \vdots \\ 0_{3\times1} & 0_{3\times1} & \cdots & \hat{b} \end{bmatrix} \tag{15}$$

where $\hat{b} = \begin{bmatrix} 0 & 0 & 1 \end{bmatrix}'$. The linear model is useful for doing analysis about robustness, stability and sensitivity. Most of the simulations however are done with the nonlinear model since it depicts the real system. The nonlinear model is of the form:

$$\dot{x} = \widetilde{A}x + Bu + P(x) \tag{16}$$

where $P(x)$ contains the nonlinearities and couplings, B is the same matrix as above and $\widetilde{A}$ is:

$$\begin{bmatrix} 0 & 1 & 0 & & 0 & 0 & 0 \\ \widetilde{a}_{21} & -b & 0 & \cdots & 0 & 0 & 0 \\ 0 & 0 & 0 & & 0 & 0 & 0 \\ & \vdots & & \ddots & & \vdots & \\ 0 & 0 & 0 & & 0 & 1 & 0 \\ 0 & 0 & 0 & \cdots & \widetilde{a}_{21} & -b & 0 \\ 0 & 0 & 0 & & 0 & 0 & 0 \end{bmatrix}$$

with $\widetilde{a}_{21} = -\omega^2 - 2C_3$.

3 Controller Design

In the previous sections the development of the spatially invariant, high-density microcantilever array model was presented. The tracking of each cantilever is important for the scanning performance of the AFM. In this paper the main control goal is therefore the cantilever's good tracking of a given sinusoidal reference signal. Up to certain reference frequencies this aim can be achieved with state feedback controllers like a decentralized velocity-feedforward controller, that consists of a PID controller with a negative feedback, supported by a positive feedforward component from the derivative of the reference or LQ optimal, localized control. A more complicated H_∞ control designed based on robust control theory in [12] is however necessary for higher, spatially varying frequencies.

3.1 Feedforward Controller

In this section a PID plus feedforward controller is presented. Each cantilever has its own local controller and each controller is fully decentralized, i.e. it only uses the information from its own cantilever. The gains of the PID controller and the feedforward gain are adjusted for the best performance. The PID control is the most common form of feedback control and is quite useful in setpoint tracking. In addition to this it is easy to implement. However, a simple PID controller may not provide enough tracking performance especially if the reference is time varying. In this case a coupling from the input signal, which can be the reference or a disturbance, is directly added to the control variable. Requiring the knowledge of system parameters and reference, this combined feedforward-feedback control can significantly improve tracking performance for time-varying reference with even high frequencies. As seen in Figure 3 the feedforward component comes from the reference and the error is a vector of differences between the displacement of the cantilevers and the reference vector. For a single cantilever the PID controller has the following formula:

$$u_{i,PID} = k_p \cdot e_i + k_d \cdot \dot{e_i} + k_i \cdot \int e_i \tag{17}$$

$$e_i = r_i - x_{i,1} \tag{18}$$

with k_p, k_d, k_i, e_i being the proportional gain, derivative gain, integral gain and the tracking error for the i_{th} cantilever respectively.

In many cases the feedforward component $F(s)$ is chosen to be the inverse of the plant transfer function $G(s)$. This makes the reference to state transfer function $(G \cdot F + G \cdot PID)/(I + G \cdot PID)$ equal to 1, meaning perfect tracking. This choice for $F(s)$

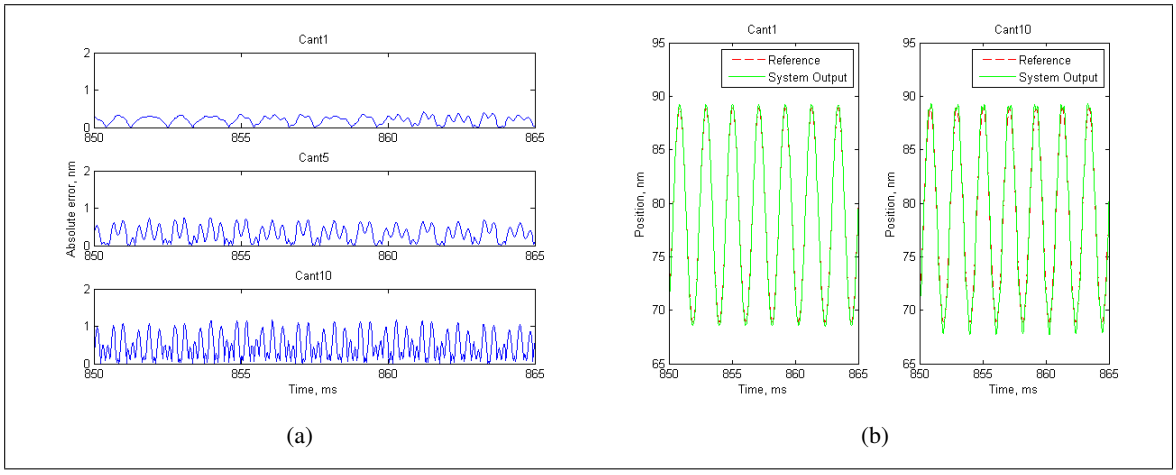

Figure 4: (a,b) Feedforward Control design: (a) Tracking error of 3 cantilevers in a system of 21 cantilevers control, (b) Reference input and tracked output for two sample cantilevers. In all the above cases the excitation frequency and amplitude are 3000rad/sec and 10nm respectively

is however not always feasible because of the non-minimum phase behavior of the plant. In addition to this, the cantilever model presented in this paper has nonlinearities and coupling effects from its neighbors which makes it harder to have an inverted transfer function of the single cantilever. Therefore, for the nonlinear cantilever array system velocity feedforward control is used with the feedforward component being the derivative of the reference scaled with a constant gain:

$$u_{i,F} = k_f \cdot \dot{r}_i \tag{19}$$

So the overall controller can be written as:

$$u = (k_p \cdot e_i + k_d \cdot \dot{e}_i + k_i \cdot \int e_i + k_f \cdot \dot{r}_i) \cdot V_1 \tag{20}$$

with V_1 being the $n \times 1$ vector consisting of only 1's, where n is the number of cantilevers. The overall controller can be designed in such way since the individual controllers do not use any neighbor information. By choosing appropriate values for the controller gains one can achieve quite satisfactory results as shown in Figure 4.

Simulations are done with a 21 cantilever-nonlinear system having the decentralized feedforward control. The reference input has a frequency of 3000 rad/sec with an amplitude of 10 nm for each cantilever. The tracking errors of cantilevers at the edges and in the middle are shown in Figure 4(a). The cantilevers have all tracking errors less than 1 nm.

Using standard tuning techniques control effort has to be kept below certain limits. The control effort in this design was always within the allowable limit of $\pm 7.5V$ [10].

3.2 Optimal State Feedback Control

In this section the controller introduced in [5] is implemented in the cantilever system. The optimal state feedback control is obtained in such a way that both the cost function, which is the tracking error in this case, and the neighbor information are minimized simultaneously. The minimizer of this constrained optimal control problem is sought using the augmented Lagrangian method. Let a linear time-invariant system be given by its state space representation

$$\begin{aligned} \dot{x} &= Ax + B_1 d + B_2 u \\ z &= \begin{bmatrix} Q^{1/2} \\ 0 \end{bmatrix} x + \begin{bmatrix} 0 \\ R^{1/2} \end{bmatrix} u \end{aligned} \tag{21}$$

where x is the state vector, d is the disturbance, u is the control input and z is the performance output. $Q^{1/2}$ and $R^{1/2}$ denote the square roots of the state and control performance weights. The structured state feedback design problem is considered

$$u = -Fx \tag{22}$$

where matrix F has to satisfy some structural constraints. Let the subspace $\mathcal{S}$ symbolize these structural constraints and let us assume that there exists a non-empty set of stabilizing F that belongs to $\mathcal{S}$. The objective is to design a control $F \in \mathcal{S}$ that minimizes H_2 norm of the transfer function from d to z. This structured optimal control problem can be formulated as an LQR type cost function $J(F)$ subject to the constraint that $F \in \mathcal{S}$. $\mathcal{S}$ in this work represents the set of matrices with having nonzero elements in the main diagonal and the immediate neighbors of the

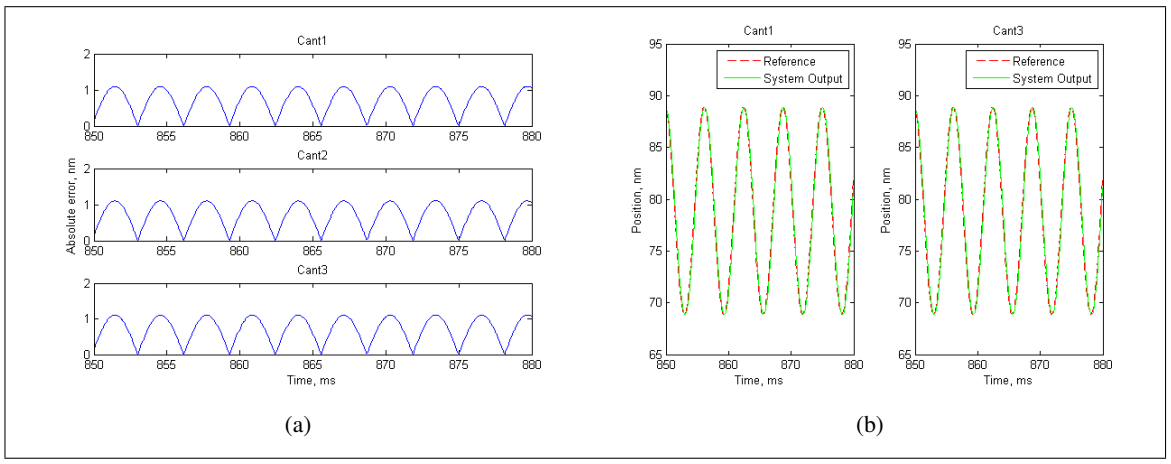

Figure 5: (a,b) LQR Control design: (a) Tracking error of 3 cantilevers in a system of 5 cantilevers, (b) Reference input and tracked output for two sample cantilevers. In all the above cases the excitation frequency and amplitude are 1000rad/sec and 10nm respectively

main diagonal only and thus having minimum possible number of nonzero elements. Hence the objective is minimizing the cost function (the H_2 norm of the reference to error transfer function) and diagonalizing F by minimizing the number of nonzero elements simultaneously, as indicated below:

$$\text{minimize} \quad J(F) + \gamma card(F) \tag{23}$$

The cardinality function $card(F)$ represents the number of nonzero elements of F. Mathematically this corresponds to a function having the value 0 for $|F_{ij}| = 0$ and a nonzero constant value (for instance 1) otherwise. γ is a non-negative number indicating the importance of sparsity of F. At $\gamma = 0$ the standard LQR problem is obtained with a centralized F as a solution. The higher the value of γ the more decentralized the controller becomes. (23) represents a strike balance between the sparsity of F and the variance amplification from d to z and this is depicted by two functions J and g. In order to decouple these functions the problem is defined in the following way:

$$\begin{aligned} &\text{minimize} \quad J(F) + \gamma g(\hat{F}) \\ &\text{subject to} \quad F - \hat{F} = 0 \end{aligned} \tag{24}$$

For the two parameters F and $\hat{F}$ a Lagrangian equation is introduced which is minimized iteratively first with respect to F then with respect to $\hat{F}$, and calculating a new Lagrange multiplier and increasing γ in each step. This iterative algorithm is called alternating direction method of multipliers (ADMM) as explained in detail in [5] and [6]. After achieving the desired level of sparsity the structured H_2 problem is solved [5] and the final controller is obtained, having a distributed structure communicating with the immediate neighbors only. For the above calculations the following software is used: www.ece.umn.edu/users/mihailo/software/lqrsp/

The minimization process starts with an optimal unstructured feedback gain F that is calculated through linear quadratic regulation. Because of the objective of having a good tracking performance rather than a mere regulation the system dynamics are augmented by an additional state q

$$q(t) = q(0) + \int_0^t (r - \hat{x}_1)dt \tag{25}$$

with r being the reference to track and x_1 being the position state. So the system dynamics are rewritten in the following way:

$$\begin{aligned} \begin{bmatrix} \dot{\hat{x}} \\ \dot{q} \end{bmatrix} &= \underbrace{\begin{bmatrix} \hat{A} & 0 \\ -C_1 & 0 \end{bmatrix}}_{A} \begin{bmatrix} \hat{x} \\ q \end{bmatrix} + \underbrace{\begin{bmatrix} 0 \\ 1 \end{bmatrix}}_{B1} r + \underbrace{\begin{bmatrix} B \\ 0 \end{bmatrix}}_{B2} u \\ \hat{x}_1 &= C_1 \hat{x} \\ u &= -F \begin{bmatrix} \hat{x} \\ q \end{bmatrix} = \begin{bmatrix} -F_x & -F_q \end{bmatrix} \begin{bmatrix} \hat{x} \\ q \end{bmatrix} \end{aligned} \tag{26}$$

The initial controller F is calculated as a solution to the linear quadratic regulation for the above problem.

The simulation results with a sample array of 5 cantilevers are shown in Figure 5. The reference signal had a frequency of 1000 rad/sec and an amplitude of 10 nm. The absolute tracking error is well below the limit of 2 nm as seen in Figure 5(b). The comparison of the tracked output of 2 sample cantilevers with

the reference input can be seen in Figure 5(a). Further simulations indicate that the control effort is around 5.5 V, similar to the feedforward control, well below the limit of 7.5 V.

3.3 H_∞-Controller

The previously presented controllers require state information which may not always be available. Furthermore, although yielding satisfactory results and being easy to implement, the feedforward controller does not guarantee good tracking or even stability for frequencies higher than 4000 rad/sec, especially when there is a phase lag, while the LQR control already has a high tracking error at a frequency of 3000 rad/sec. The H_∞ controller is another alternative for the cantilever array and is designed in such a way that it only uses the output information, meaning the current and the voltage from the cantilever. The advantage of this controller is its taking the coupling effects into consideration and its being built in a more systematic way than the feedforward control. The linear fractional transformation (LFT) setup for this control design is shown in Figure 6 with P and K representing the plant and the controller respectively. $\widehat{u}$ is the vector of integrals of control inputs u for each cantilever. z_u is the weighted rate of change of the input voltage, $z_{\widehat{u}}$ is the weighted input voltage, z_e is the weighted tracking error, r is the reference command, x_1 is the vector consisting of the microcantilever positions and finally $\widehat{w}$ and $\widehat{d}$ are the vectors of external disturbance. W_u and $W_{\widehat{u}}$ are design weights guaranteeing that the control effort doesn't exceed the allowable limit of $\pm 7.5V$ [10]. W_e, W_w, W_d are chosen to

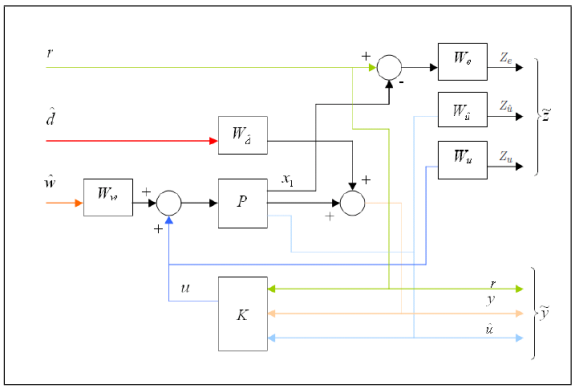

Figure 6: LFT Formulation for H_∞ Control Design [7]

control the device bandwidth, attenuate the effect of any external disturbance entering the system at the input channel and attenuate the effect of high frequency measurement noise on the system output respectively [12]. The controller is designed using an infinite Linear Spatial Time Invariant (LSTI) abstraction of the dynamics of one cantilever and the coupling from its neighbors, augmented with the above defined weights. Using the methods in [1] the spatial shift operator can be defined as $S = e^{j\theta}$ over the interval $[0\ 2\pi]$. Defining A_{big}, B_{big}, C_{big} and D_{big} as the state, input, output and feedthrough matrices of the augmented single cantilever, and assuming that the information of only 2 neighbors on each side is considerable the augmented state matrix with the shift operator can be written as

$$A_{big}(S) = A_{big-2}S^{-2} + A_{big-1}S^{-1} + A_{big} + A_{big1}S^{1} + A_{big2}S^{2} \quad (27)$$

with $S^k = e^{kj\theta}$. The gridding is then done over the Fourier frequencies θ in order to get the infinite model for the controller design. By splitting C_{big} and D_{big} into C_{big1} and D_{big1} for the output to be minimized $\tilde{z}$,and C_{big2} and D_{big2} for the output to be controlled $\tilde{y}$ the following state equations for the infinite approximation of the augmented cantilever dynamics are obtained

$$\begin{aligned}\dot{\hat{x}} &= A_{big}(S)\cdot\hat{x} + B_{big}\cdot\begin{bmatrix}\hat{w} & \hat{d} & r & u\end{bmatrix}'\\ \tilde{z} &= C_{big1}\cdot\hat{x} + D_{big1}\cdot\begin{bmatrix}\hat{w} & \hat{d} & r & u\end{bmatrix}'\\ \tilde{y} &= C_{big2}\cdot\hat{x} + D_{big2}\cdot\begin{bmatrix}\hat{w} & \hat{d} & r & u\end{bmatrix}'\end{aligned} \quad (28)$$

From here one can obtain the state equations of the H_∞ controller:

$$\begin{aligned}\dot{x}_k &= A_k(S)x_k + B_k(S)y\\ u &= C_k(S)x_k + D_k(S)y\end{aligned}$$

Each of the matrices of the above equation of the controller can be written in the same manner as in (27). As an example the state matrix $A_k(S)$ with 2 neighbors on each side is presented

$$A_k(S) = A_{k-2}S^{-2} + A_{k-1}S^{-1} + A_{k0} \quad (29)$$
$$+ A_{k1}S^{1} + A_{k2}S^{2} \quad (30)$$

The coefficient matrices A_{ki} can be determined using Least Square Estimation (LSE). Let n denote the dimension of the matrix $A_k(S)$ and $A_k(i)$ the value of the operator $A_k(S)$ at the i_{th} gridding point of the Fourier frequency θ

$$\begin{aligned}A_k(i) &= I_n e^{-2j\theta}, I_n e^{-j\theta}, I_n, I_n e^{j\theta}, I_n e^{2j\theta})\\ &\times (A_{k-2}, A_{k-1}, A_{k0}, A_{k1}, A_{k2})^* \quad (31)\\ &:= \psi_i \times \Omega\end{aligned}$$

In the above equation ψ_i can be easily calculated and $A_k(S) =$ is known. So for all the gridding points i the following equation can be written

$$\begin{bmatrix} A_k(1) \\ A_k(2) \\ \vdots \\ A_k(m) \end{bmatrix} = \begin{bmatrix} \psi_1 \\ \psi_2 \\ \vdots \\ \psi_m \end{bmatrix} \Omega$$
$$or \tag{32}$$
$$A_k = \Phi \times \Omega$$

where m is the number of the gridding points of Fourier frequencies θ. Using LSE theorem in [7], one of the best coefficient matrix estimates is given by

$$\Omega = [(Re\Phi)'(Re\Phi) + (Im\Phi)'(Im\Phi)]^{-1} \cdot \begin{bmatrix} Re\Phi \\ Im\Phi \end{bmatrix}' \begin{bmatrix} ReA_k \\ ImA_k \end{bmatrix} \tag{33}$$

with Re being the real part and Im being the imaginary part. The same calculations are done for $B_k(S)$, $C_k(S)$ and $D_k(S)$ and one obtains the distributed H_∞ controller

$$\begin{aligned} \dot{x}_k &= A_k x_k + B_k y_k \\ u_k &= C_k x_k + D_k y_k \end{aligned} \tag{34}$$

with the structure

$$\begin{aligned} \dot{x}_k &= [A_{k-2}S^{-2} + \ldots + A_{k0} + \ldots + A_{k2}S^2]x_k \\ &+ [B_{k-2}S^{-2} + \ldots + B_{k0} + \ldots + B_{k2}S^2]y_k \\ u_k &= [C_{k-2}S^{-2} + \ldots + C_{k0} + \ldots + C_{k2}S^2]x_k \\ &+ [D_{k-2}S^{-2} + \ldots + D_{k0} + \ldots + D_{k2}S^2]y_k \end{aligned} \tag{35}$$

or in matrix form

$$A_k = \begin{pmatrix} a_{k0} & a_{k1} & 0 & \cdots & 0 \\ a_{k1} & a_{k0} & a_{k1} & \cdots & 0 \\ \vdots & & \ddots & & 0 \\ 0 & \cdots & 0 & a_{k1} & a_{k0} \end{pmatrix} \tag{36}$$

where a_{k0}, a_{k1} are submatrices of the controller obtained from the above mentioned controller design. The Figure 7 shows the results of the simulations performed with a sample array of 5 cantilevers and the reference signal having a frequency of 3000 rad/sec and an amplitude of 10 nm. The comparison between the reference input and the tracked output of 2 cantilevers is presented in Figure 7(b). The absolute tracking error for each cantilever, shown in Figure 7(a) is below 2 nm that is the acceptable limit. Because of the lack of the state information the results are slightly worse than that of the feedforward controller in Figure 4 where the absolute error is always below 1nm. With a value below 3.5 V the control effort required for the H_∞ controller however is lower than the one for the state feedback controllers.

4 Multimodal Modeling

The performance and robustness analysis with various controllers was done so far with a simplified model of the cantilever array where each cantilever was viewed as one dynamical unit having only 3 states, namely its position, velocity and the voltage applied on it. However in reality the cantilever is not a point mass but has a more complicated structure instead. Therefore in order to have a more accurate analysis on the control performance the further complexities of the cantilever system have to be taken into account. Multimodal modeling, or finite element method particularly, cuts the structure into several elements, creates dynamical equations for each element and describes the equations of a single cantilever by combining them. As shown in Figure 8 each cantilever is assumed to consist of n beam elements, resulting in $n + 1$ position points. Each position point has a vertical displacement and also a rotation of the beam at the point associated with it. Thus each cantilever has $2 \cdot (n + 1)$ states:

$$\bar{z}_i = \begin{bmatrix} x_{i,v,1} \\ x_{i,\theta,1} \\ x_{i,v,2} \\ x_{i,\theta,2} \\ \vdots \\ x_{i,v,n+1} \\ x_{i,\theta,n+1} \end{bmatrix} \tag{37}$$

with v representing the vertical and θ the rotational displacement. $\bar{z}_i$ is the displacement vector of the i_{th} cantilever.

The FEM model uses a base matrix for each beam element with

$$K_1 = \frac{EI}{h^3} \cdot \begin{bmatrix} 12 & 6h & -12 & 6h \\ 6h & 4h^2 & -6h & 2h^2 \\ -12 & -6h & 12 & -6h \\ 6h & 2h^2 & -6h & 4h^2 \end{bmatrix} \tag{38}$$

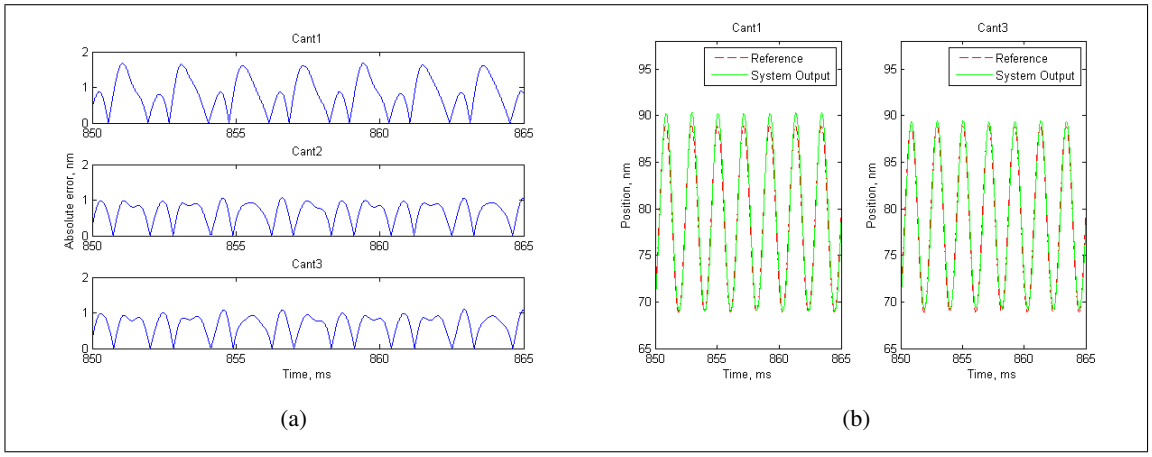

Figure 7: (a,b) H_∞ control design: (a) Tracking error of 3 cantilevers in a system of 5 cantilevers, (b) Reference input and tracked output for two sample cantilevers. In all the above cases the excitation frequency and amplitude are 3000rad/sec and 10nm respectively

as the base stiffness matrix and

$$M_1 = \frac{\rho A_r h}{420} \cdot \begin{bmatrix} 156 & 22h & 54 & -13h \\ 22h & 4h^2 & 13h & -3h^2 \\ 54 & 13h & 156 & -22h \\ -13h & -3h^2 & -22h & 4h^2 \end{bmatrix} \quad (39)$$

as the base mass matrix [13]. These matrices are derived from the principal of virtual work by assuming a cubic interpolation function for the displacements. E signifies the Young's modulus, I the area moment of inertia about the z-axis, h the element length ρ the density and A_r the cross-section area. The matrices in (38) and (39) are used to produce the beam mass matrix M and beam stiffness matrix K for each cantilever. These are created in a pattern where the base submatrix is placed in the top left corner and the next submatrix is placed diagonal to the previous location, shifted two down and two across. The M and K matrices are used in the basic characteristic equation of the form:

$$M\ddot{x} = -Kx \quad (40)$$

The mass matrix can be moved to the other side to give us the solution to cantilever system

$$\ddot{x} = -M^{-1}Kx = (M\_K)x \quad (41)$$

where M_K is a $(2n+2) \times (2n+2)$ single mass-stiffness matrix for one cantilever. To make sure the attached end of the cantilever is rigid the first and second rows and columns are zeroed, meaning that the cantilever position at the attached end cannot change. The obtained M_K matrix is used in the modified characteristic equation of the cantilever system.

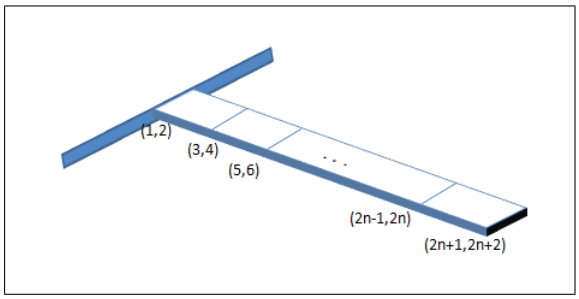

Figure 8: Multimodal model of the cantilever beam

Because $x_{i,1}$ of the i_{th} cantilever is measured at the tip the vertical displacement of the last beam element and the corresponding velocity are used for coupling calculations and the calculation of the current: $x_{i,1} = x_{i,v,n+1} = \bar{z}_i(2n+1)$ and $x_{i,2} = \dot{x}_{i,v,n+1} = \dot{\bar{z}}_i(2n+1)$. Assuming the equilibrium values of $\bar{z}_i$, $\dot{\bar{z}}_i$ and V_i given by $\bar{z}_e$, 0, V_e respectively the following definitions are made: $\bar{x}_{1i} = \bar{z}_i - \bar{z}_e$, $\bar{x}_{2i} = \dot{\bar{z}}_i$, $\bar{x}_{3i} = V_i - Ve$. The modified state space equations of the multimodal cantilever can now be written:

$$\begin{aligned} \dot{\bar{x}}_{1i} &= \bar{x}_{2i} \\ \dot{\bar{x}}_{2i} &= (M\_K)\bar{x}_{1i} - b\bar{x}_{2i} + F_{total,i}P \\ \dot{\bar{x}}_{3i} &= u \end{aligned} \quad (42)$$

where P is a $(2n+2) \times 1$ vector with $P(2n+1) = 1$ and the other elements of the vector being 0. $F_{total,i}$ is the sum of all the forces acting on the $i'th$ cantilever:

$$F_{total,i} = F_{a,i} + F_{mech,i} + F_{elec,i}^{\perp} \quad (43)$$

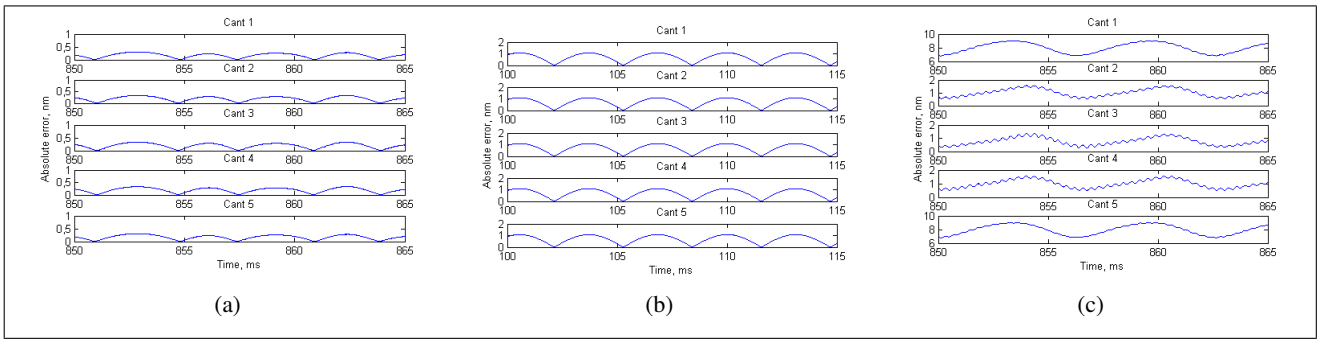

Figure 9: (a,b,c) Control design with FEM Model: (a) Tracking error of 5 cantilevers with Feedforward Control, (b) Tracking error of 5 cantilevers with LQR Control, (c) Tracking error of 5 cantilevers with H_∞ Control. In all the above cases the excitation frequency and amplitude are 1000rad/sec and 10nm respectively

Figure 9 compares the absolute tracking errors of 5 cantilevers with the feedforward control in Figure 9(a), LQR control in Figure 9(b) and H_∞ control in Figure 9(c). The simulations are done with 5 cantilevers, the reference input having a frequency of 1000 rad/sec and an amplitude of 10 nm, and the results are similar to that for the simple model. According to Figure 9(a) the absolute tracking error remains below 1 nm if the feedforward controller is used and it is below 2 nm for the LQR control. Similarly in the H_∞ control the absolute tracking error is below 2 nm for all but the edge cantilevers, as shown in Figure 9(b). From the operational point of view the edge cantilevers can be neglected; meaning that the output feedback H_∞ controller attains the performance of the state feedback controller, even for the FEM model. However the satisfactory tracking performances for the FEM model are achieved at the expense of high control effort; nearly 20 V for the feedforward control, 18 V for the LQR control and nearly 15 V for the H_∞ control

5 Stability and Robustness

The previous sections show that the presented controllers yield satisfactory results with tracking errors within acceptable limits, up to a reference frequency of 3000 rad/sec. The sensitivity analysis is an important tool to further determine performance and robustness characteristics of the design. The bandwidth of the Bode plot of reference to error transfer function is a good indicator for this. In order to have the full information of the cantilever system the singular value plots are drawn for the feedforward, the LQR and the H_∞ controllers in Figure 10 in an array of 5 cantilevers. The LQR controller has clearly a lower bandwidth of between 12000-14000 rad/sec, similar to the feedforward controller, whereas the bandwidth for the H_∞ control is around 30000 rad/sec.

A similar analysis can be done with the LSTI infinite abstraction that is introduced in Section 3. The A matrix of a single cantilever in an array of infinitely many cantilevers can be written as:

$$A = ... + A_{-2}S^{-2} + A_{-1}S^{-1} + A_0 + A_1S^1 + A_2S^2... \quad (44)$$

with S as the spatial shift operator associated with coupling from neighbors. A good LSTI model can be obtained by using only a 2 neighbor interaction. In this case the A matrix in a spatial Fourier transform representation would be:

$$A(\theta) = A_{-2}e^{-2j\theta} + A_{-1}e^{-j\theta} + A_0 + A_1e^{j\theta} + A_2e^{2j\theta} \quad (45)$$

with θ being the spatial frequency. The same LSTI infinite abstraction was also applied to the H_∞ controller. Figure 11 shows the resulting reference to error Bode plot for the feedforward controller, Figure 12 the one for the LQR and finally Figure 13 shows the one for the H_∞ controller, using various values of the spatial frequency θ. All of them yield very similar results to the singular value plots of Figure 10. So a finite system with a high number of cantilevers is not expected to lead to any different analysis.

The above analysis shows that the H_∞ controller should be working significantly better at high reference frequencies. The numerical experiments show that at a frequency of 4500 rad/sec the maximum absolute tracking error is 2 nm for the H_∞ controller and the feedforward controller, the one of the LQR controller is however already above 3 nm. At higher

frequencies all controllers perform worse with the performance of the LQR and feedforward controllers deteriorating faster. The feedforward control may even become unstable for frequencies higher than 5000 rad/sec. Although the LQR controller yields higher absolute tracking errors both the LQR and the H_∞ controllers remain stable even at frequencies as high as 50000 rad/sec.

A traditional way of analyzing the stability robustness of a system is calculating its phase and gain margins. Phase margin is the amount of additional phase lag at the gain crossover frequency required to make the system unstable and gain margin is the additional loop gain causing instability. For a stability analysis both of them have to be calculated. The LQR control system's open loop transfer function has a phase margin of 60 degrees and its gain margin is 7.35 dB. The closed loop system is stable since both of the values are positive and desirable. Similarly the H_∞ control has open loop phase and gain margins of 60.4 degrees and 11.1 dB respectively. These results imply that phase shifts or change of some parameters do not bring the system in the verge of instability, which is also verified by simulations. The feedforward controller on the other hand has phase and gain margins of 9.53 degrees and 7.25 dB. While the gain margin has an acceptable value the relatively low phase margin indicates that the closed loop system is more sensitive to phase shifts, as verified by simulations. Note that these results are also compatible with the much higher peak value of the reference to error Bode plot of the feedforward control than the LQR and H_∞ controllers in Figure 10 since the high H_∞ norm of the sensitivity function would indicate poor robustness of the system.

The results of the FEM model are also analyzed in the frequency domain. The reference to displacement plots of the simple and FEM models with the feedforward controller can be seen in Figure 14. Matching to the complementary sensitivity plot of the simple model for low frequencies and having peaks only at higher frequencies, the complementary sensitivity plot of the FEM model shows that the feedforward control is applicable on the FEM model and would yield results similar to the ones of the simple model for frequencies until 6000 rad/sec.

Figure 15 shows the reference to displacement bode plots of both the simple and the FEM model, using the LQR controller. The bandwidth of the FEM model has a value of around 6000 rad/sec however there are no extra peaks; meaning the LQR controller developed from the simple model can be implemented on the FEM model without having a significant performance degradation in terms of tracking, stability or robustness.

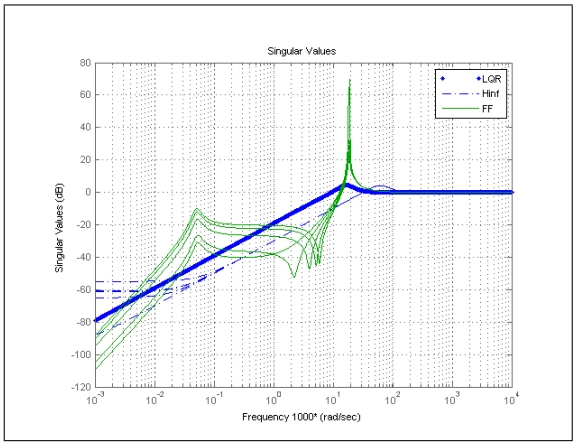

Figure 10: Singular value plots of reference to error transfer function for an array of 5 cantilevers using Feedforward Control, LQR Control and H_∞ Control (magnitude in dB, frequency in $10^3 rad/sec$)

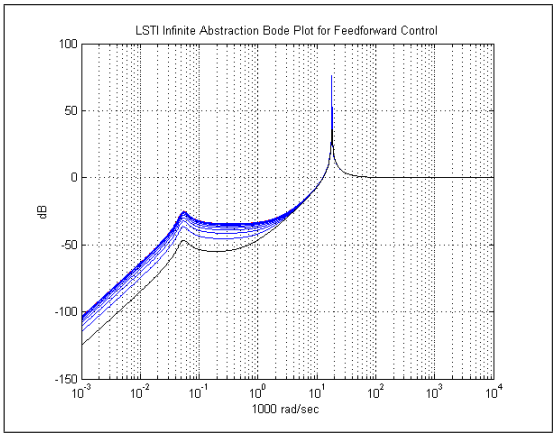

Figure 11: LSTI infinite abstraction bode magnitude plot of reference to error transfer function for one cantilever using Feedforward Control (red for $\theta = 0$, black for $\theta = 2\pi$, magnitude in dB, frequency in $10^3 rad/sec$)

The reference to displacement bode plot of the simple and FEM models using the distributed H_∞ control can be seen in Figure 16. Both plots match at frequencies up until 6000 rad/sec, however the one for the FEM model starts to deteriorate at higher frequencies with having high peaks. This means that the implementation of the H_∞ controller from the simple model on the FEM model would not yield a setback in terms of tracking, stability or robustness for frequencies lower than 6000 rad/sec, a degradation however may occur for higher frequencies.

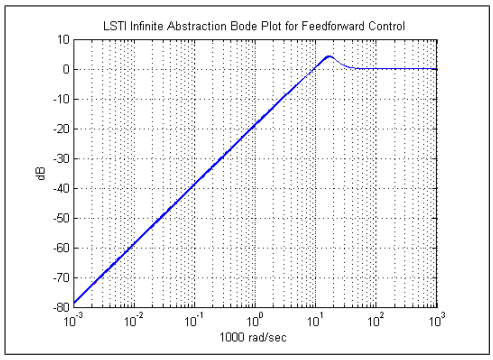

Figure 12: LSTI infinite abstraction bode magnitude plot of reference to error transfer function for one cantilever using LQR Control (red for $\theta = 0$, black for $\theta = 2\pi$, magnitude in dB, frequency in $10^3 rad/sec$)

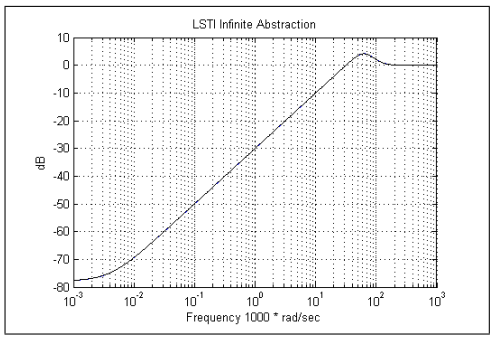

Figure 13: LSTI infinite abstraction Bode magnitude plot of reference to error transfer function for one cantilever using H_∞ Control

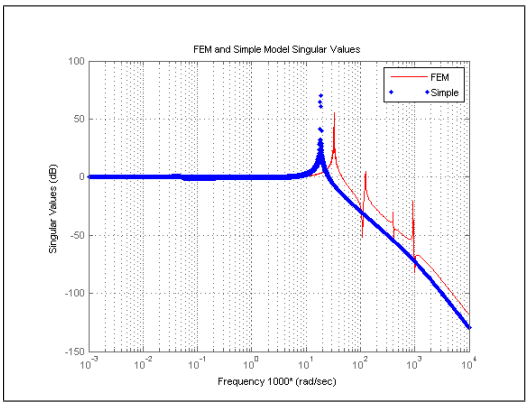

Figure 14: Reference to displacement singular value plot of the closed loop systems of simple model and FEM. Feedforward controller is used.

6 Conclusion

In this paper alternative controllers to the H_∞ control were presented for two different models of an infinite array of electrostatically actuated microcantilevers. The cantilevers have weak mechanical and electrostatic couplings where only 3-4 neighbors on each side make any significant contribution. Furthermore the dynamics of the cantilevers do not change along a spatial axis, meaning that the system is spatially invariant.

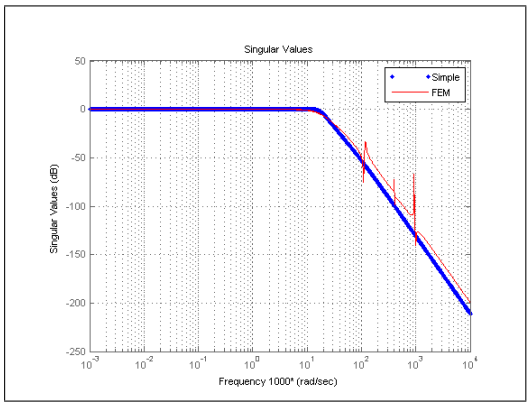

Figure 15: Reference to displacement singular value plot of the closed loop systems of simple model and FEM. LQR controller is used.

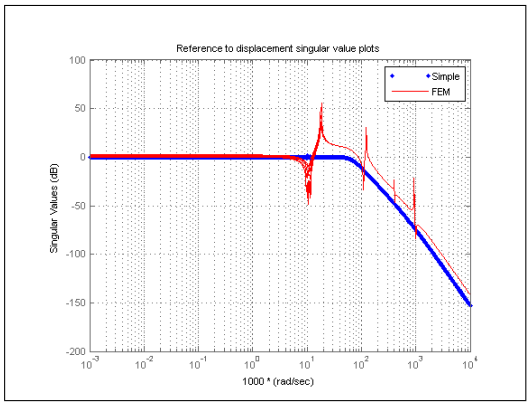

Figure 16: Reference to displacement singular value plot of the closed loop systems of simple model and FEM. H_∞ controller is used.

The modeling of the cantilever was performed in 2 different ways. The first one was a simple nonlinear model where each cantilever was considered as a point mass with its displacement, velocity and voltage being the only states, whereas the second one was a multimodal model that considers each cantilever as a more complex structure consisting of smaller segments each of which has rotational and vertical displacements and velocities as their states. For the successful actuation of the cantilevers 2 types of controllers were developed and implemented, the first type being the state feedback and the second type being the output feedback. All of the controllers were designed from the linearization of the simple nonlinear model.

The first state feedback controller is a PID controller having additionally a velocity feedforward component from the reference. It is a fully decentral-

ized controller and designed by adjusting the weights for the best performance. Although it yields a resolution of less than 1 nm at frequencies as high as 3000 nm for the simple nonlinear model, given that the same excitation frequency is used across the array, the tracking error may increase up to 10 nm if the excitation frequency is changed. Frequency analysis and simulations furthermore indicate that the tracking performance may deteriorate at higher frequencies. Because of these downsides of the feedforward controller an optimal state feedback controller from [5] was introduced next. The LQR type controller, that was designed by simultaneous localization and optimization, has a distributed structure where each controller communicates with the immediate neighbors only. This controller is robust in comparison to the feedforward controller and yields acceptable results at excitation frequencies up to 2000 rad/sec according to the simulations with the simple nonlinear model, even if the frequency is varied across the array. However it does not provide enough resolution at higher frequencies without excessive control.

The analysis with the FEM model also verified the above results. The state feedback controllers hence may be a vital alternative in cases where the excitation frequencies are not too high or they do not vary significantly across the array and when the state information is available. In more general cases, however, the output feedback H_∞ controller is more suitable for the high density microcantilever array system, as demonstrated in this paper. The distributed controller, localized for each cantilever and communicating only with immediate neighbors, can attain a quite desired performance with a tracking error less than 2 nm up to excitation frequencies of 3000 rad/sec, low tracking errors at varying frequencies and higher frequency bandwidths than the state feedback controllers. This result can also be observed in the analysis with the FEM model, where except for the edge cantilevers, which can be neglected from an operational point of view, the tracking error remains below 2 nm for the distributed controller at a frequency up to 1000 rad/sec; however at the expense of higher control effort and lower bandwidth of the sensitivity function.

In conclusion, the state feedback controllers with the feedforward or LQR structures may be significant alternatives for the high density cantilever array. Their implementation is not complicated, require less calculation time and provide satisfactory results. However the distributed H_∞ controller is the most appropriate one for spatially and temporally invariant array systems especially when the states are not measurable. Future work can be directed towards more comprehensive robustness analysis, experiments with the existing controllers and further investigation of the LQR control from [5].

Acknowledgements: This work has been supported by a Fellowship from the National Center of Supercomputing Applications at the University of Illinois and by the National Science Foundation [Grant NSF ECCS 10-27437].

References:

[1] B. Bamieh, F. Paganini and M. Dahleh, Distributed Control of spatially invariant systems. *IEEE Transactions on Automatic Control* 47, 2002, pp. 1091–1107.

[2] M. Despont, J. Brugger, U. Drechsler, et al., VLSI-NEMS chip for parallel AFM data storage. *Sensors and Actuators A: Physical* 80, 2000, pp. 100–107.

[3] R. Garcia and R. Perez, Dynamic Atomic Force Microscopy Methods. *Surface Science Reports* 47, 2002, pp. 197–301.

[4] F. Giessibl, Advances in Atomic Force Microscopy. *Rev. of Modern Physics* 75, 2003, pp. 950–983.

[5] F. Lin, M. Fardad and M. Jovanovic, Design of optimal sparse feedback gains via the alternating direction method of multipliers. *IEEE Transactions on Automatic Control*, 58, 2011, pp. 2426–2431.

[6] F. Lin, M. Fardad and M. Jovanovic, Sparse feedback synthesis via the alternating direction method of multipliers. *Proceedings of the 2012 American Control Conference*, 2012, pp. 4765–4770.

[7] L. Ljung, *System Identification: Theory for the User*. Englewood Cliffs, Prentice Hall, Inc, New Jersey, 1987.

[8] B. Mehmet, *Modeling and Control of High Density Microcantilever Systems*. MS Thesis, University of Illinois at Urbana Champaign, Urbana, Illinois, 2012.

[9] A. Moulin, S. O'Shea and M. Welland, Microcantilever-based biosensors. *Ultramicroscopy* 82, 2000, pp. 23–31.

[10] M. Napoli, B. Bamieh and K. Turner, A capacitive microcantilever: Modeling, validaton and estimation using current measurements. *ASME Journal of Dynamical Systems Measurement and Control* 126, 2004, pp. 319–326.

[11] A. Sarwar, *Modelling and Control of Electrostatically Actuated Microcantilever Array*. MS Thesis, University of Illinois at Urbana Champaign, Urbana, Illinois, 2006.

[12] A. Sarwar, P. Voulgaris and S. Salapaka, On the control design and robustness analysis for high-density microcantilever arrays. *Journal of Vibration and Control* 17, 2011, pp. 1195–1210.

[13] G. Sauer and M. Wolf, A Modified Beam Element Mass Matrix. *Zeitschrift für angewandte Mathematik und Mechanik* 68, 1988, pp. 483–490.

[14] E. Wachter, T. Thunat, P. Oden, et al., Remote optical detection using microcantilevers. *Review of Scientific Instruments* 67, 1996 pp. 3434–3439.

[15] W. Zhou, A. Khaliq, Y. Tang, et al., Simulation and design of piezoelectric microcantilever chemical sensors. *Sensors and Actuators A: Physical* 125, 2005, pp. 69–75.